Optimized Pulse Patterns for Anisotropic Synchronous Machines

Eleftherios Kontodinas*, Petros Karamanakos*, Andreas Kraemer†, and Sebastian Wendel†
*Faculty of Information Technology and Communication Sciences, Tampere University, 33101 Tampere, Finland
Email: *eleftherios.kontodinas@tuni.fi, p.karamanakos@ieee.org
†ZF Friedrichshafen AG, 97424 Schweinfurt, Germany
Email: †andreas.kraemer@zf.com, sebastian.wendel@zf.com

***Abstract*—Advanced optimized pulse patterns (OPPs) that account for the magnetic anisotropy of permanent magnet synchronous motors (PMSMs) have recently gained the attention of the automotive industry due to the improvements they offer in the current quality. However, these improvements can lead to torque quality degradation and an increased dc-link current ripple. To address this problem, a hybrid modulation scheme that combines isotropic and anisotropic OPPs is proposed in this paper to achieve the best overall performance over the whole range of operating points. To do so, as shown with the presented results, different OPPs are assessed and those with the best overall performance are selected.**

I. Introduction

The increasing demand for efficient drivetrains in the automotive industry has led to the adoption of sophisticated synchronous modulation methods, such as optimized pulse patterns (OPPs). Assuming a purely inductive load, traditional OPPs are computed such that they produce the minimum harmonic distortions at a given switching frequency [1]. Owing to this feature, traditional OPPs bring additional objectives, such as increased system efficiency, as shown in [2] for low-voltage three-phase interior permanent magnet synchronous motors (IPMSMs) used in electric vehicles.

To further improve the performance of traditional OPPs in terms of current harmonic distortions, the operating point-dependent magnetic anisotropy of IPMSM drives can be taken into account in the optimization procedure [3]–[6]. To do so, the harmonic content of an anisotropic PMSM is properly captured in the objective function. More specifically, the optimization problem becomes a function of the modulation index, the load angle, and the saliency ratio. Moreover, half-wave symmetry (HWS) can be imposed to extend the solution space. As shown in the aforementioned work, by doing so, the margin for harmonic content reduction is significantly improved once anisotropy is taken into account.

However, the OPPs applied to the converter do not only affect the quality of the current but also the electromagnetic torque. Especially at high speeds, where the OPPs are mostly used, the low-order current is quite high, leading to significant low-order harmonics in the electromagnetic torque [7]. These harmonics can cause, in turn, significant speed ripples, mechanical vibrations, and additional losses [8]. For these reasons, OPPs for propulsion applications—where new requirements such as smoother torque and lower vibrations are constantly proposed—should be assessed not only for the produced current quality but also for the resulted torque harmonics.

Besides the effect on the torque, OPPs that minimize the phase current ripple while accounting for the anisotropy of the machine may also lead to an increased dc-link current ripple, see [9]. This increases the temperature/loses and accelerates the wear-out of the dc-link capacitor. The latter becomes vital in electric vehicles, where the usage of several capacitors is not an option due to the limited available space and additional cost arising. Hence, the effect of OPPs on the dc-link current ripple needs to be taken into account as well.

Considering the above, and given that in practical applications the performance of the system must meet specific requirements, the effect of modulation methods, such as OPPs, need to be assessed not only based on the stator current quality but also other factors, such as the electromagnetic torque and dc-link current ripples. Motivated by this, this work assesses isotropic and anisotropic OPPs with different symmetry properties based on different performance metrics. As shown, the performance of the OPPs heavily depends on the operating point, with no single type of OPPs being optimal for the entire operating region. To address this, modulation maps are derived that show the type of OPPs with the lowest current distortions at each operating point while meeting specific application requirements. These modulation maps can be subsequently used when operating the IPMSM drive system such that the most favorable type of OPPs is selected at each given operating point, thus maximizing the system performance.

II. OPPs for Anisotropic Motors

A. Two-Level Pulse Patterns

The automotive drive system considered in this work consists of a two-level inverter and an IPMSM (see Fig. 1). Assuming a (constant) dc-link voltage V_{dc}, the inverter produces a switched voltage in each phase $x \in \{a, b, c\}$ that assumes two values, namely $V_{\mathrm{dc}}/2$ when the corresponding switch position is $u_x = 1$, and $-V_{\mathrm{dc}}/2$ when $u_x = -1$. Considering that the waveform $u \equiv u_a$ has a period of 2π, then the number of pulses in one period is $q = f_{\mathrm{sw}}/f_1 \in \mathbb{N}^+$, where f_{sw} and f_1 are the switching and the fundamental frequency, respectively. This implies that if the switched waveform u has quarter-

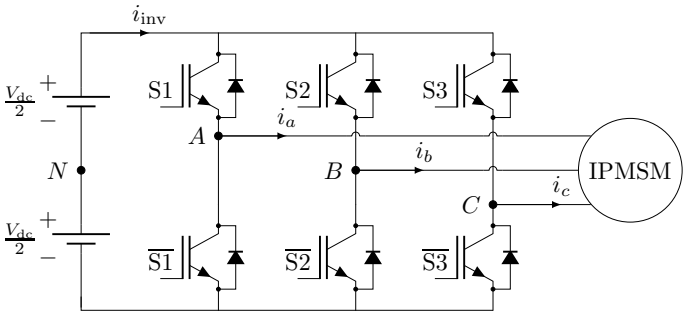

Fig. 1: Electrical drive system consisting of a two-level inverter and an IPMSM.

and half-wave symmetry (QaHWS), there are $d = (q-1)/2$ switching events in one quarter of the full period.

As shown in [1] and [3], when relaxing the symmetry of the switched waveform from QaHWS to half-wave symmetry (HWS), the current quality can be improved. This is due to the additional degrees of freedom, as instead of the d switching angles (i.e., time instants) that can be manipulated when QaHWS is concerned, $2d+1$ angles can be manipulated, see Fig. 2. Given this, the Fourier coefficients of a HWS two-level switched waveform are given by

$$a_0 = 0 \tag{1}$$

$$a_n = \begin{cases} 0, & n = 2,4,6,\dots \\ -u_0 \frac{4}{n\pi} \sum_{i=1}^{2d+1} (-1)^i \sin(n\alpha_i), & n = 1,3,5,7,\dots \end{cases} \tag{2}$$

$$b_n = \begin{cases} 0, & n = 2,4,6,\dots \\ u_0 \frac{4}{n\pi} \sum_{i=1}^{2d+1} (-1)^i \cos(n\alpha_i), & n = 1,3,5,7,\dots . \end{cases} \tag{3}$$

Note that HWS still eliminates the even harmonics as well as the dc component, while the phase of the fundamental sinusoidal component can be zero, i.e., $a_1 = 0$ $b_1 = m$, where m is the desired modulation index.

B. Stator Voltage in Rotating Reference Frame

When the computation of OPPs accounts for the anisotropy of the machine, it is necessary to derive the formulations of the motor current in a rotating reference frame as a function of the switching angles of the pulse pattern. To this end, the dq-reference frame is employed that rotates counterclockwise with the synchronous angular speed ω_s.[1] The initial angle between the d-axis of the dq-frame and the α-axis of the orthogonal stationary ($\alpha\beta$) frame is denoted with $\theta_{r,0}$. Finally, for the purposes of the analysis that follows, the rotor flux vector $\boldsymbol{\psi}_r$ is aligned with the d-axis, see Fig. 3(a). In the same figure, the stator voltage vector $\boldsymbol{v}_s$—which corresponds to the vector of the applied pulse pattern—is also depicted. The phase of $\boldsymbol{v}_s$ is $\theta_{\boldsymbol{v}_s} + \phi_c$, where $\theta_{\boldsymbol{v}_s} = \arctan(a_1/b_1)$ and ϕ_c is the initial displacement of the Fourier coefficients axes. Note that the latter are shown with red lines and indicate the

[1]Note that as IPMSMs are considered in this work, the rotor speed ω_r is equal to the synchronous speed ω_s.

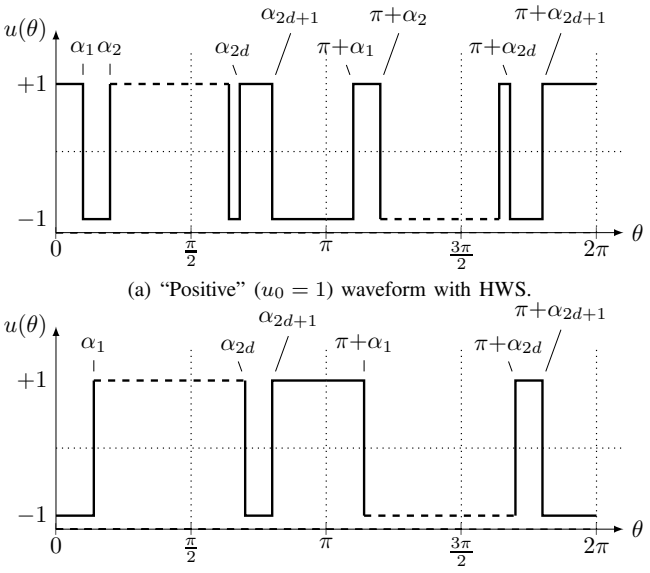

(a) "Positive" ($u_0 = 1$) waveform with HWS.

(b) "Negative" ($u_0 = -1$) waveform with HWS.

Fig. 2: Two-level switched waveform with HWS.

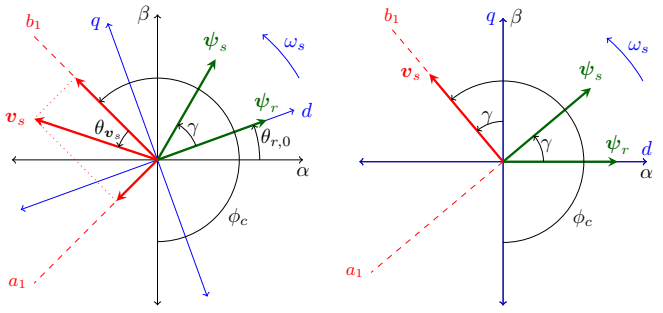

(a) General representation ($t = 0$) (b) Representation after assumptions

Fig. 3: Vector diagram of an IPMSM.

position of the a_1 and b_1 Fourier coefficients. Finally, γ is the load angle.

The optimization problem is solved for $a_1 = 0$ and $b_1 = m$, meaning that $\boldsymbol{v}_s$ is aligned with the axis of the b_1 Fourier coefficient, and $\theta_{\boldsymbol{v}_s} = 0$. Moreover, R_s is considered very small compared to the inductive part of the machine, hence it can be neglected, i.e., $R_s \approx 0$. This means the stator voltage vector is perpendicular to the stator flux vector $\boldsymbol{\psi}_s$. Finally, by assuming that the d-axis is initially aligned with the α-axis, i.e., $\theta_{r,0} = 0$, the angle ϕ_c becomes $\phi_c = \gamma + \pi$, see Fig. 3(b).

Given the above and the electrical rotor position $\theta_r = \omega_s t$, the Fourier representation of the HWS single-phase inverter output voltage—which is equal to the stator voltage—is

$$v_s(\theta_r + \phi_c) = \frac{V_{\text{dc}}}{2} \sum_{n=1}^{\infty} a_n \cos(n\theta_r + n\phi_c) + b_n \sin(n\theta_r + n\phi_c)\,, \tag{4}$$

where the single-phase voltage v_{sx} depends on the single-phase pulse pattern u_x according to $v_{sx} = \frac{V_{\text{dc}}}{2} u_x$. To transform the three-phase stator voltage $\boldsymbol{v}_{s,abc} = [v_{sa}\ v_{sb}\ v_{sc}]^T$ from the abc- to the dq-frame the Park transformation is employed, i.e., $\boldsymbol{v}_{s,dq} = \boldsymbol{R}(\theta_r)\boldsymbol{K}\boldsymbol{v}_{s,abc}$, where

$$\boldsymbol{R}(\theta_r)=\begin{bmatrix}\cos(\theta_r) & \sin(\theta_r)\\ -\sin(\theta_r) & \cos(\theta_r)\end{bmatrix},\quad \boldsymbol{K}=\frac{2}{3}\begin{bmatrix}1 & -\frac{1}{2} & -\frac{1}{2}\\ 0 & \frac{\sqrt{3}}{2} & -\frac{\sqrt{3}}{2}\end{bmatrix}.$$

It is noteworthy that due to the reference frame transformation the order of the stator voltage harmonics in the dq-reference is a multiple of six, i.e., $n=6k$, where $k\in\mathbb{N}$, whereas the voltage harmonics in the abc-frame are at odd and non-triplen multiples of the fundamental frequency, i.e., $n=6k\pm1$.

C. Stator Current in Rotating Reference Frame

The time-domain voltage equations of an IPMSM in the dq-frame are

$$v_{sd}=R_s i_{sd}+X_{sd}\frac{\mathrm{d}i_{sd}}{\mathrm{d}t}-\omega_s X_{sq} i_{sq} \tag{5a}$$

$$v_{sq}=R_s i_{sq}+X_{sq}\frac{\mathrm{d}i_{sq}}{\mathrm{d}t}+\omega_s X_{sd} i_{sd}+\omega_s\psi_{\mathrm{PM}}\,, \tag{5b}$$

where $\boldsymbol{v}_{s,dq}=[v_{sd}\ v_{sq}]^T$ is the stator voltage, $\boldsymbol{i}_{s,dq}=[i_{sd}\ i_{sq}]^T$ the stator current, X_{sd} and X_{sq} the inductances on the d- and q-axis, respectively, and ψ_{PM} the PM flux. Finally, note that a sinusoidal back-electromotive force (back-EMF) is assumed.

Transforming (5) into the frequency domain yields

$$\begin{bmatrix}v_{sd}\\ v_{sq}-\omega_s\psi_{\mathrm{PM}}\end{bmatrix}=\begin{bmatrix}R_s+sX_{sd} & -\omega_s X_{sq}\\ \omega_s X_{sd} & R_s+sX_{sq}\end{bmatrix}\begin{bmatrix}i_{sd}\\ i_{sq}\end{bmatrix}, \tag{6}$$

with $s=\jmath n\omega_s$. This expression, in turn, can be written as

$$\begin{bmatrix}i_{sd}\\ i_{sq}\end{bmatrix}=\begin{bmatrix}R_s+sX_{sd} & -\omega_s X_{sq}\\ \omega_s X_{sd} & R_s+sX_{sq}\end{bmatrix}^{-1}\begin{bmatrix}v_{sd}\\ v_{sq}-\omega_s\psi_{\mathrm{PM}}\end{bmatrix}. \tag{7}$$

Hence, the harmonic (i.e., $n>0$) current frequency response is

$$\begin{bmatrix}i_{sd,n}\\ i_{sq,n}\end{bmatrix}=\begin{bmatrix}R_s+sX_{sd} & -\omega_s X_{sq}\\ \omega_s X_{sd} & R_s+sX_{sq}\end{bmatrix}^{-1}\begin{bmatrix}v_{sd,n}\\ v_{sq,n}\end{bmatrix}. \tag{8}$$

With (8), the harmonic current in the abc-frame can be computed. To this end, the inverse Park transformation is employed, i.e., $\boldsymbol{i}_{s,abc}=\boldsymbol{K}^{-1}\boldsymbol{R}^{-1}(\theta_r)\boldsymbol{i}_{s,dq}$. Note that owing to (8), the derived single-phase current accounts for the magnetic anisotropy. Specifically, by introducing the saliency ratio $\chi=X_{sq}/X_{sd}$, and with the help of (4), the magnitude of the phase current for positive-sequence harmonics is

$$\hat{i}_{sa,n^+}=\frac{V_{\mathrm{dc}}}{4\omega_s X_{sq}}\left(\left(\frac{a_n}{n}(\chi{+}1)+\frac{a_{n-2}}{n-2}(\chi{-}1)\cos(2\gamma)-\frac{b_{n-2}}{n-2}(\chi{-}1)\sin(2\gamma)\right)^2+\left(-\frac{b_n}{n}(\chi{+}1)-\frac{b_{n-2}}{n-2}(\chi{-}1)\cos(2\gamma)-\frac{a_{n-2}}{n-2}(\chi{-}1)\sin(2\gamma)\right)^2\right)^{\frac{1}{2}} \tag{9}$$

while that of negative-sequence harmonics is

$$\hat{i}_{sa,n^-}=\frac{V_{\mathrm{dc}}}{4\omega_s X_{sq}}\left(\left(\frac{a_n}{n}(\chi{+}1)+\frac{a_{n+2}}{n+2}(\chi{-}1)\cos(2\gamma)+\frac{b_{n+2}}{n+2}(\chi{-}1)\sin(2\gamma)\right)^2+\left(-\frac{b_n}{n}(\chi{+}1)-\frac{b_{n+2}}{n+2}(\chi{-}1)\cos(2\gamma)+\frac{a_{n+2}}{n+2}(\chi{-}1)\sin(2\gamma)\right)^2\right)^{\frac{1}{2}}. \tag{10}$$

III. OPP Optimization Problem

Stator currents with low harmonic distortions can result in lower iron and copper losses, and thus thermal losses, in the machine. To quantify the harmonic content of the stator current, the total demand distortion (TDD) given by

$$I_{s,\mathrm{TDD}}=\frac{1}{\sqrt{2}I_{s,\mathrm{nom}}}\sqrt{\sum_{n\neq1}\hat{i}_{s,n}}^2=\frac{1}{\sqrt{2}I_{s,\mathrm{nom}}}\sqrt{\sum_{n=7,13,\ldots}(\hat{i}_{sa,n^+})^2+\sum_{n=5,11,\ldots}(\hat{i}_{sa,n^-})^2}. \tag{11}$$

is typically employed. Therefore, when the aim is to compute OPPs that minimize the current distortions, the following objective function can be considered

$$\begin{aligned}J(\boldsymbol{\alpha})=&\sum_{n=6k}^{\infty}\left(\left(\frac{a_{n+1}}{n+1}\right)^2+\left(\frac{b_{n+1}}{n+1}\right)^2\right)\frac{\chi^2+1}{2}\\&+\sum_{n=6k}^{\infty}\left(\left(\frac{a_{n-1}}{n-1}\right)^2+\left(\frac{b_{n-1}}{n-1}\right)^2\right)\frac{\chi^2+1}{2}\\&+\sum_{n=6k}^{\infty}\left(\frac{a_{n-1}}{n-1}\frac{a_{n+1}}{n+1}+\frac{b_{n-1}}{n-1}\frac{b_{n+1}}{n+1}\right)(\chi^2-1)\cos(2\gamma)\\&+\sum_{n=6k}^{\infty}\left(\frac{a_{n-1}}{n-1}\frac{b_{n+1}}{n+1}-\frac{a_{n+1}}{n+1}\frac{b_{n-1}}{n-1}\right)(\chi^2-1)\sin(2\gamma)\,,\end{aligned} \tag{12}$$

where (9) and (10) are used, while the scaling factor in (11) is omitted as it does not affect the optimization process.

With (12), the optimization problem that computes HWS OPPs that account for the anisotropy of the machine can be formulated as

$$\underset{\boldsymbol{\alpha}\in[0,\pi]^{2d+1}}{\text{minimize}}\quad J(\boldsymbol{\alpha}) \tag{13a}$$

$$\text{subject to}\quad -u_0\frac{4}{\pi}\sum_{i=1}^{2d+1}(-1)^i\sin(\alpha_i)=0 \tag{13b}$$

$$u_0\frac{4}{\pi}\sum_{i=1}^{2d+1}(-1)^i\cos(\alpha_i)=m \tag{13c}$$

$$0\leq\alpha_1\leq\alpha_2\cdots\leq\alpha_{2d+1}\leq\pi\,, \tag{13d}$$

where the constraint (13b) imposes zero initial phase on the fundamental sinusoidal component, and (13c) guarantees that the desired modulation index $m\in[0,\,4/\pi]$ is synthesized.

TABLE I: Parameters of the IPMSM drive system

Parameter	Value	Parameter	Value
Nominal voltage V_N	926 V	Nominal frequency f_1	120 Hz
Nominal current I_N	138 A	Pole pairs	4
Nominal power P_N	190 kW	Dc-link voltage $V_{\rm dc}$	800 V
Stator resistance R_s	0.046 Ω	Power factor	0.86
d-axis inductance L_{sd}	1.58 mH	PM flux linkage $\lambda_{\rm PM}$	0.684 Wb
q-axis inductance L_{sq}	6.48 mH		

Moreover, the inequality constraints (13d) ensure that the optimal switching angles are in an ascending order and within the interval $[0,\, \pi]$ due to the HWS of the OPP. Finally, it is worth mentioning that the optimization procedure is repeated for each combination of modulation index m, load angle γ, and saliency ratio χ, which increases the computational burden required for the computation of such OPPs.

IV. Performance Evaluation of OPPs

As can be deduced from (13), the OPPs are computed by targeting the lowest possible current TDD, while neglecting the torque TDD and dc-link current ripple. As a result, it is necessary to evaluate the overall performance of a given OPP to gain insight into its impact on the torque and dc-link current ripple. To this end, four different types of OPPs are assessed in this section, namely (a) isotropic OPPs with QaHWS (isoQaHWS OPPs), (b) isotropic OPPs with HWS (isoHWS OPPs), (c) anisotropic OPPs with QaHWS (anisoQaHWS OPPs), and (d) anisotropic OPPs with HWS (anisoHWS OPPs). These OPPs are applied to the IPMSM drive system (see Fig. 1) with the parameters shown in Table I, and their performance is assessed under different operating points.

A. Performance Metrics

To assess the steady-state performance of the drive system with the four aforementioned types of OPPs, three different metrics are adopted, namely, the stator current TDD ($I_{s,\rm TDD}$), the torque TDD ($T_{\rm TDD}$), and the dc-link current TDD ($I_{\rm inv,TDD}$). With regards to the first metric, i.e., $I_{s,\rm TDD}$, its analytical expression is provided in (11).

As for the torque TDD, the electromagnetic torque is

$$T_e = ((X_{sd} - X_{sq})i_{sd} + \psi_{\rm PM})i_{sq} \tag{14}$$

where $\boldsymbol{i}_{s,dq}$ can be calculated from (7). Hence, the torque harmonics amplitude is computed by applying Fourier analysis to (14) and the torque $T_{\rm TDD}$ can be calculated according to

$$T_{\rm TDD} = \frac{1}{T_{e,\rm nom}} \sqrt{\sum_{n\neq 0} \hat{T}_{e,n}}^{2} . \tag{15}$$

Finally, the inverter dc-link current $i_{\rm inv}$ (Fig. 1) is given by

$$i_{\rm inv} = (\boldsymbol{s}_{abc})^T \boldsymbol{i}_{s,abc} \tag{16}$$

where $\boldsymbol{s}_{abc}$ is the switching state of the upper switches of the inverter, i.e., $s_x = 0$ if the upper switch of phase $x \in \{a, b, c\}$ is open, and $s_x = 1$ if it is closed. Therefore, given the three-phase OPP $\boldsymbol{u}_{abc}$, $\boldsymbol{s}_{abc}$ can be computed with

$$\boldsymbol{s}_{abc} = \frac{\mathbf{1}_3 + \boldsymbol{u}_{abc}}{2} , \tag{17}$$

where $\mathbf{1}_3$ is a three-dimensional vector of ones. Therefore, $i_{\rm inv}$ is computed based on (17) and the (known) three-phase current $\boldsymbol{i}_{s,abc}$. Hence, the corresponding TDD $I_{\rm inv,TDD}$ can be derived by using Fourier transformation of the dc-link current waveform.

B. Methodology

For a meaningful assessment that provides the necessary insight into which OPP type is most suitable for a given operating point, a wide range of comparisons is performed in this section. More specifically, isotropic HWS, anisotropic QaHWS, and anisotropic HWS OPPs are benchmarked against traditional OPPs, i.e., isotropic QaHWS OPPs, in terms of the performance metrics introduced in Section IV-A. In doing so, the improvement/deterioration of the overall system performance due to the symmetry relaxations and inclusion of the anisotropy into the optimization problem can be assessed. The comparisons are done for torque in the range $T_e \in [0, 1.2]$ per unit (p.u.) and over the whole range of achievable modulation indices, i.e., $m \in [0,\, 4/\pi]$. For the performed tests, a motor with a fixed saliency ratio ($\chi = 4.1$) is considered (see Table I). Finally, for comparison purposes, the relative TDD values are introduced as

$$\zeta_{\rm TDD,rel}(\xi) = \frac{\zeta_{\rm TDD}(\xi) - \zeta_{\rm TDD}(\text{isoQWS})}{\zeta_{\rm TDD}(\text{isoQWS})} \cdot 100\% \tag{18}$$

where

- $\zeta \in \{I_s, T, I_{\rm inv}\}$
- and $\xi \in \{\text{isoHWS, anisoQWS, anisoHWS}\}$.

The relative performance metrics of the above-mentioned comparisons are presented in Fig. 4 for $d = 4$. With regards to the isotropic HWS OPPs, it can be observed that, in general, they result in a lower or equal stator current TDD compared with that of isotropic QaHWS OPPs, see Fig. 4(a). However, this improvement usually comes at a cost of a worse torque TDD. Particularly, as can be seen in Fig. 4(d), the $T_{\rm TDD}$ deteriorates in the operating region with the most significant $I_{s,\rm TDD,rel}$ reduction.

On the other hand, anisotropic OPPs always result in a better stator current TDD than the isotropic QaHWS OPPs. Alas, the increase in the torque TDD is significant in the low-torque region, where the current TDD gain is the highest, see Figs. 4(e) and 4(f). Moreover, when focusing on the QaHWS anisotropic OPPs, it can be seen that the quality of the stator current is either minutely better or the same as that of isotropic QaHWS OPPs in the area where the torque is improved (see Figs. 4(b) and 4(e)). As for the dc-link current ripple, this also mostly benefits when OPPs account for the anisotropy of the machine, see Figs. 4(h) and 4(i). Nevertheless, it is worth noting that there are operating points with an increase in $I_{\rm inv,TDD,rel}$ of up to 15% in the low-torque region.

When assessing the impact of the symmetry relaxation, it can be seen that the improvement of $I_{\rm s,TDD,rel}$ becomes more prominent and reaches up to 47%. However, HWS compromises the torque TDD as it is mostly equal or worse than that of isotropic QaHWS OPPs, see Figs. 4(a) and 4(f).

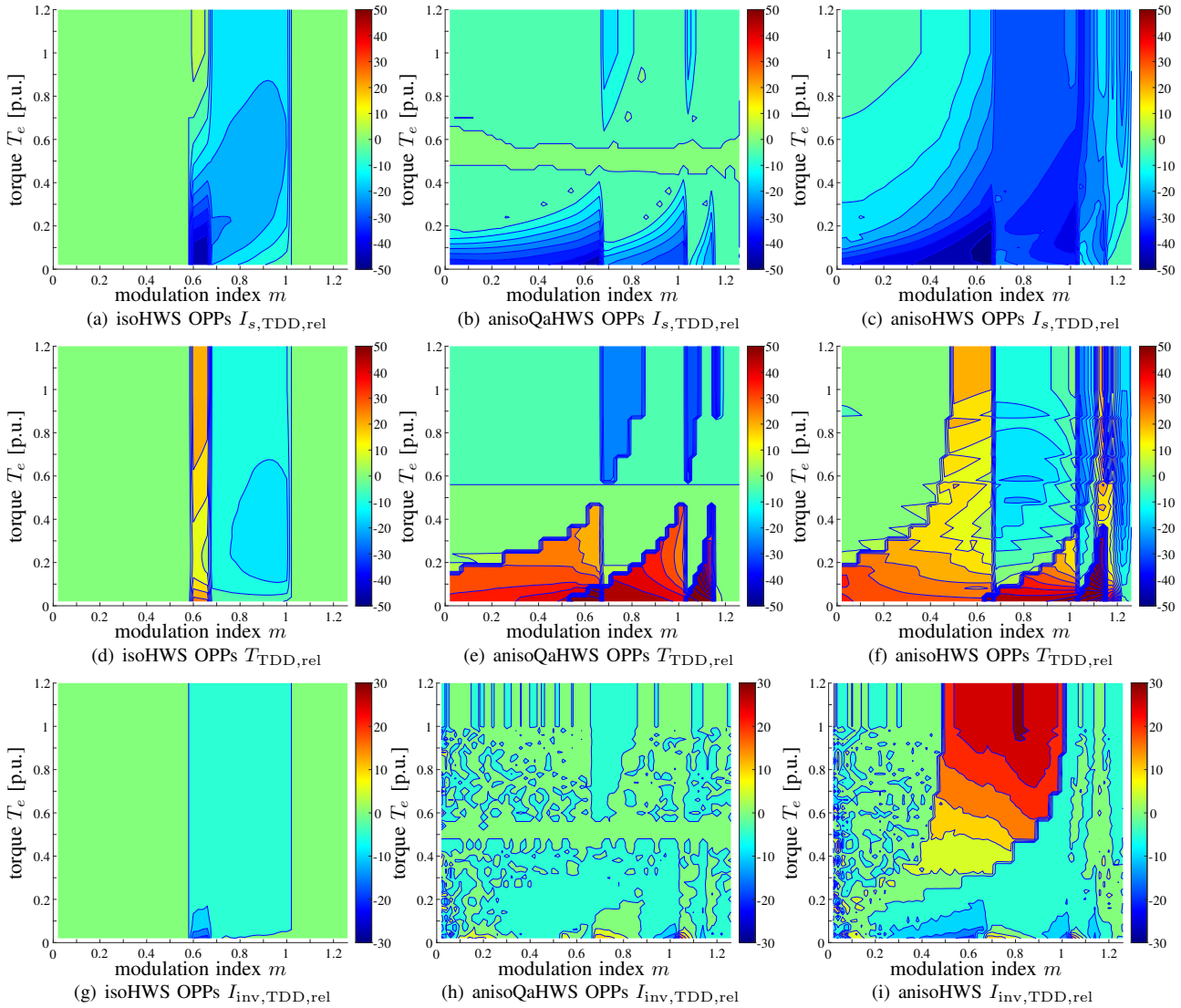

(a) isoHWS OPPs $I_{s,\mathrm{TDD,rel}}$ (b) anisoQaHWS OPPs $I_{s,\mathrm{TDD,rel}}$ (c) anisoHWS OPPs $I_{s,\mathrm{TDD,rel}}$

(d) isoHWS OPPs $T_{\mathrm{TDD,rel}}$ (e) anisoQaHWS OPPs $T_{\mathrm{TDD,rel}}$ (f) anisoHWS OPPs $T_{\mathrm{TDD,rel}}$

(g) isoHWS OPPs $I_{\mathrm{inv,TDD,rel}}$ (h) anisoQaHWS OPPs $I_{\mathrm{inv,TDD,rel}}$ (i) anisoHWS $I_{\mathrm{inv,TDD,rel}}$

Fig. 4: Relative performance metrics of isoHWS, anisoQaHWS, and anisoHWS OPPs with respect to isoQaHWS OPPs for $d = 4$.

Moreover, anisoHWS OPPs do not limit the deterioration of the dc-link current quality to the operating points in the low-torque region. As can be observed in Fig. 4(i), for modulation indices in the range $[0.4, 1]$ and mid- to high-torque, there is an increase in $I_{\mathrm{inv,TDD,rel}}$ that should be considered in the OPPs selection since it can be up to 30%.

C. OPP Selection Maps

The performance of different types of OPPs varies significantly from one operating point to another when the targeted motor has magnetic anisotropy. That makes the selection of the most suitable OPP quite complicated. To facilitate the OPP selection, performance criteria should be defined based on which the OPP that maximizes the drive performance at each operating point is selected. Nevertheless, it is important to point out that the results of such an approach heavily depend on the drive itself and the chosen requirements.

Given the above, the following procedure can be adopted to generate OPP maps, where the "optimal" pattern is indicated at each operating point. First, isoQWS OPPs are chosen as the base patterns for all operating points. Following, a different type of OPP is chosen when it meets the following criteria at the same time:

- it has lower $I_{s,\mathrm{TDD}}$ than the isoQaWS OPPs, i.e., $I_{s,\mathrm{TDD,rel}} < 0\%$;
- it has lower T_{TDD} than the isoQaWS OPPs or worse up to a tolerance of T_{tol}, i.e., $T_{\mathrm{TDD,rel}} < T_{\mathrm{tol}}$;
- and it has lower $I_{\mathrm{inv,tol}}$ than the isoQaHWS OPPs or worse up to a tolerance of $I_{\mathrm{inv,tol}}$, i.e., $I_{\mathrm{inv,TDD,rel}} < I_{\mathrm{inv,tol}}$.

If at least one criterion is not met, then isoQWS remains the pattern of preference in that specific operating point. In the last step, if more than one pattern meets the aforementioned criteria at an operating point, the OPP with the lowest $I_{s,\mathrm{TDD}}$ is preferred.

With the introduced approach, Fig. 5 presents the OPP selection map for $d = 4$ when zero tolerance in torque and dc-link current relative TDD is allowed. As can be seen, by not allowing any deterioration in torque and dc-link current

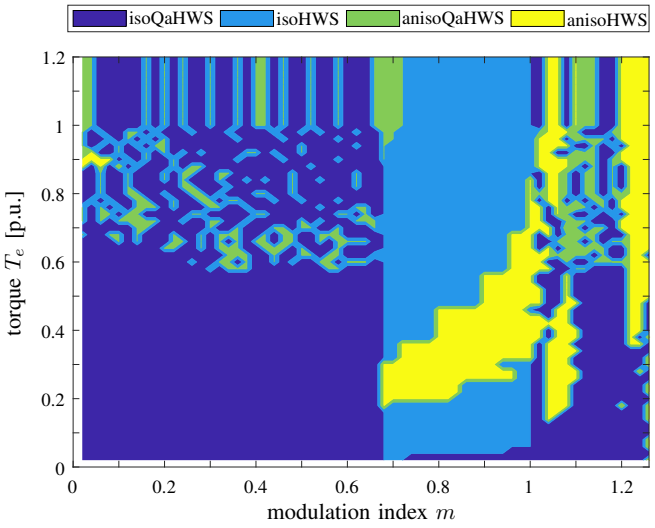

Fig. 5: OPP map for $d = 4$ with $T_{\text{tol}} = 0\%$ and $I_{\text{inv,tol}} = 0\%$.

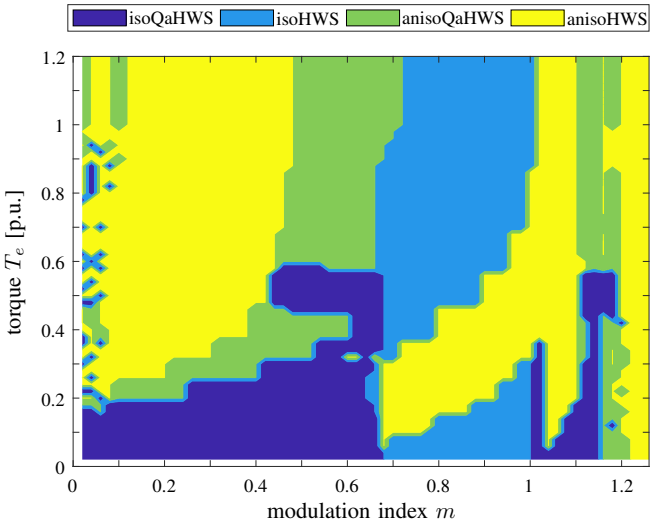

Fig. 6: OPP map for $d = 4$ with $T_{\text{tol}} = 10\%$ and $I_{\text{inv,tol}} = 5\%$.

ripple, the OPP type that is suitable in most cases is the isotropic OPPs with QaHWS. Nonetheless, for modulation indices between 0.7 and 1 the isotropic HWS OPPs are mostly preferred as they result in better performance. In the same region, there is also an area where anisotropic HWS OPPs are beneficial. On the other hand, anisotropic OPPs with QaHWS are used only in the high-torque region but only intermittently due to increased dc-link ripple. Based on the map shown in Fig. 5, it can be concluded that the zero-tolerance policy can be seen as too restrictive as it indicates that isotropic QaHWS OPPs are the most favorable type.

To further reduce the harmonic losses of the drive system, a 10% tolerance in $T_{\text{TDD,rel}}$ increase is introduced along with a 5% tolerance in $I_{\text{inv,TDD,rel}}$ increase. The OPP map that corresponds to these new criteria is shown in Fig. 6. As can be observed, when relaxing the improvement requirements in T_{TDD} and $I_{\text{inv,TDD}}$, anisotropic OPPs—either with QaHWS or HWS—are employed for most of the operating points. This is thanks to the much lower stator current TDD they produce, which enables an increase in the IPMSM drive efficiency. On the other hand, isotropic QaHWS OPPs, even if they have the worst $I_{s,\text{TDD}}$ compared with the rest of OPP types, are still the most suitable for low-torque and modulation indices (i.e., $m \in [0, 0.7]$) due to the lower torque ripples.

Based on the above, it can be claimed that the generated OPP maps show the most favorable OPPs depending on the criteria defined by the automotive industry for a given application. As a result, the most favorable drive performance can be ensured as the benefits accredited to OPPs are fully exploited.

V. Conclusion

In this paper, different types of OPPs for PMSMs with magnetic anisotropy were derived and assessed in detail. In doing so, the impact of the anisotropic properties of a PMSM on the performance of isotropic and anisotropic OPPs was investigated. The presented results indicated that when the anisotropy of the machine is accounted for in the optimization process the current TDD can be significantly improved. This, however, can come at the expense of increased torque and dc-link current ripples. To address this, OPP maps were derived based on defined criteria to visualize the beneficial areas of each OPP type. Hence, these maps facilitate the selection of the most favorable OPP type that leads to the best "overall" performance at each operating point.

Acknowledgment

This work was supported in part by ZF Friedrichshafen AG and in part by the Academy of Finland.

References

[1] A. Birth, T. Geyer, H. d. T. Mouton, and M. Dorfling, "Generalized three-level optimal pulse patterns with lower harmonic distortion," *IEEE Trans. Power Electron.*, vol. 35, no. 6, pp. 5741–5752, Jun. 2020.

[2] E. Kontodinas, A. Kraemer, H.-D. Endres, S. Wendel, P. Karamanakos, and J. Bonifacio, "An experimental assessment of modulation methods for drive trains used in electric vehicles," in *Proc. IEEE Ind. Electron. Conf.*, Brussels, Belgium, Oct. 2022, pp. 1–6.

[3] A. Birda, J. Reuss, and C. M. Hackl, "Synchronous optimal pulsewidth modulation for synchronous machines with highly operating point dependent magnetic anisotropy," *IEEE Trans. Ind. Electron.*, vol. 68, no. 5, pp. 3760–3769, May 2021.

[4] Z. Zhang, X. Ge, Z. Tian, X. Zhang, Q. Tang, and X. Feng, "A PWM for minimum current harmonic distortion in metro traction PMSM with saliency ratio and load angle constrains," *IEEE Trans. Power Electron.*, vol. 33, no. 5, pp. 4498–4511, May 2018.

[5] N. Hartgenbusch, R. W. De Doncker, and A. Thünen, "Optimized pulse patterns for salient synchronous machines," in *Proc. Int. Conf. Elect. Mach. and Syst.*, Hamamatsu, Japan, Nov. 2020, pp. 359–364.

[6] G. Darivianakis and I. Tsoumas, "Insight into the peculiarities of optimized pulse patterns for permanent-magnet synchronous machines," in *Proc. Eur. Conf. on Power Electron. and Applicat.*, Lyon, France, Sep. 2020, pp. P.1–P.8.

[7] S. D. T. Robertson and K. M. Hebbar, "Torque pulsations in induction motors with inverter drives," *IEEE Trans. Ind. and Gen. Appl.*, vol. IGA-7, no. 2, pp. 318–323, Mar. 1971.

[8] G. Feng, C. Lai, X. Tan, B. Wang, and N. C. Kar, "Optimal current modeling and identification for fast and efficient torque ripple minimization of PMSM using theoretical and experimental models," *IEEE Trans. Ind. Electron.*, vol. 68, no. 12, pp. 11 806–11 816, Dec. 2021.

[9] A. Birda, C. Grabher, C. M. Hackl, and J. Reuss, "Dc-link capacitor and inverter current ripples in anisotropic synchronous motor drives produced by synchronous optimal PWM," *IEEE Trans. Ind. Electron.*, vol. 69, no. 5, pp. 4484–4494, May 2022.